J. Fluid Mech. (2007), *vol.* 573, *pp.* 1–25.
doi:10.1017/S002211200600351X Printed in the United Kingdom

Simulation of cavitation bubbles in a convergent–divergent nozzle water jet

Z. QIN[1,2], K. BREMHORST[3], H. ALEHOSSEIN[4] AND T. MEYER[1,2]

[1]Division of Mining and Minerals Process Engineering, The University of Queensland, Brisbane, QLD, Australia, 4072

[2]CRCMining, The University of Queensland, Brisbane, QLD, Australia, 4072

[3]Division of Mechanical Engineering, The University of Queensland, Brisbane, QLD, Australia, 4072

[4]CSIRO Exploration and Mining, Brisbane, Queensland 4069, Australia

(Received 16 May 2005 and in revised form 28 June 2006)

A model for simulating the process of growth, collapse and rebound of a cavitation bubble travelling along the flow through a convergent–divergent nozzle producing a cavitating water jet is established. The model is based on the Rayleigh–Plesset bubble dynamics equation using as inputs ambient pressure and velocity profiles calculated with the aid of computational fluid dynamics (CFD) flow modelling. A variable time-step technique is applied to solve the highly nonlinear second-order differential equation. This technique successfully solves the Rayleigh–Plesset equation for wide ranges of pressure variation and bubble original size and saves considerable computing time. Inputs for this model are the pressure and velocity data from CFD calculation. To simulate accurately the process of bubble growth, collapse and rebound, a heat transfer model, which includes the effects of conduction plus radiation, is developed to describe the thermodynamics of the incondensable gas inside the bubble. This heat transfer model matches previously published experimental data well. Assuming that single bubble behaviour also applies to bubble clouds, the calculated distance from the nozzle exit travelled by the bubble to the point where the bubble size becomes invisible is taken to be equal to the bubble cloud length observed. The predictions are compared with experiments carried out in a cavitation cell and show good agreement for different nozzles operating at different pressure conditions.

1. Introduction

In cavitating water jets which are submerged in water, cavitation bubbles form and collapse and travel along the jet. When the bubbles reach a solid target, the target is eroded owing to the collapse of the bubbles. Figure 1 is a schematic of a cavitating water jet generated by a convergent–divergent nozzle where bubbles are growing and collapsing in the flow stream. Experimental results of the cavitating water jet revealed a strong connection between the length of a bubble cloud and the erosion ability of a water jet (Qin 2004). To predict the behaviour of a cavitating water jet, we must study the process of bubble formation, travel and collapse. The most important aspect of cavitation theory is the bubble dynamics which was originated by Rayleigh (1917). He studied the mechanics and physics of the formation and collapse of a bubble by ignoring surface tension and viscous effects. This theory was subsequently amended by others (Plesset 1949; Knapp, Daily & Hammit 1970; Lauterborn & Bolle 1975; Young 1989; Shima *et al.* 1989; Prosperetti 1994).

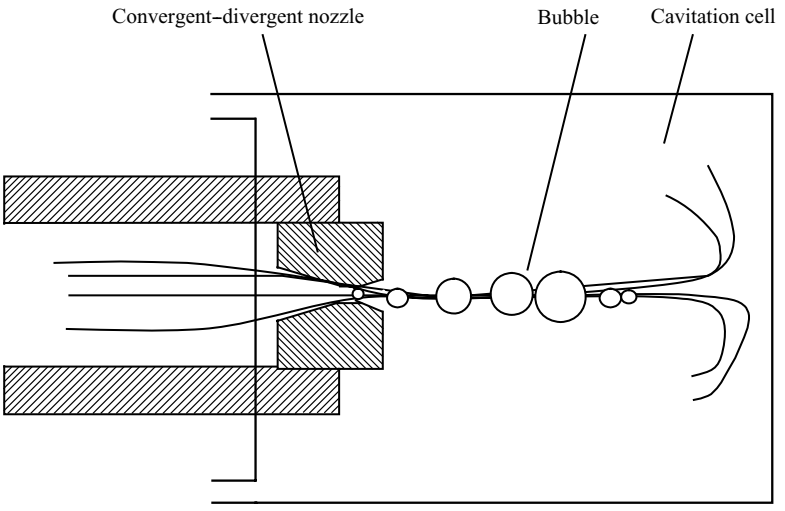

FIGURE 1. Schematic diagram of a cavitating water jet.

Plesset (1949) applied Rayleigh's equation to the problem of travelling cavitation bubbles. Knapp (1952) showed a comparison of Rayleigh's theory with experimental results. However, because of the difficulties in obtaining pressure fields outside and inside the bubble, many workers can use only the assumed pressure values to simulate the bubble growth and collapse; hence, the results obtained can provide only a qualitative explanation for the cavitation phenomenon. Since the cavitation phenomenon in a cavitating water jet is typically the reflection of the growth, travel, collapse and rebound of bubbles experiencing variable external pressures, in order to study the bubble behaviour, we must obtain information on pressure variation in the water jet flow. With the advance of computational fluid dynamics (CFD), the pressure field along a jet flow can be calculated. Qin (2004) studied the flow properties including the profiles of pressure, velocity and turbulent kinetic energy in water-jet flow using CFD by comparing various turbulence models with experiments. The study revealed that there is a substantial pressure reduction in the throat of a convergent–divergent nozzle flow, which helps explain the mechanism of cavitation formation. The flow properties calculated from CFD provide the possibility for simulating accurately the bubble behaviour in a water jet. The major aim of this paper is to establish a proper model to simulate the process of the growth and collapse of a bubble when it flows through a convergent–divergent nozzle, so as to predict how far the bubble can travel before it completely collapses. Such a model provides the basis for predicting the erosion on a solid target located downstream.

The modelling is based on solving the Rayleigh–Plesset equation involving determination of the pressure variations inside and outside the bubble, as well as the selection of a numerical method. The finite-difference method is used to solve the Rayleigh–Plesset differential equation. The inputs for the model are the profiles of pressure and velocity calculated using the commercial CFD code, FLUENT. Since the Rayleigh–Plesset equation is highly nonlinear, any numerical scheme with constant time step is not able to simulate the whole process of the bubble collapse, especially the final stage of collapse when the range of pressure variation that the bubble experiences is large. To handle the large pressure variation, a numerical method with variable time steps is developed which allows simulation of the violent process of

the final stage of the bubble collapse. To describe this process, a thermal model is developed which reflects the heat transfer. The results from the model are compared with those from experiments.

2. Rayleigh–Plesset equation for a spherical bubble

Consider a spherical bubble of radius R, as a function of time t, in an infinite domain of liquid. If the temperature in the domain is constant and the liquid is incompressible, the generalized Rayleigh–Plesset equation describing the motion of the bubble wall is (Brennen 1995):

$$\rho\left[R\frac{\mathrm{d}^2R}{\mathrm{d}t^2}+\frac{3}{2}\left(\frac{\mathrm{d}R}{\mathrm{d}t}\right)^2\right]=p_B-p_\infty-\frac{2\sigma}{R}-\frac{4\mu}{R}\frac{\mathrm{d}R}{\mathrm{d}t}, \tag{1}$$

where σ and μ represent the surface tension and viscosity of the liquid, p_B is the pressure inside the bubble and p_∞ is the pressure of the liquid surrounding the bubble. Given p_∞, equation (1) can be solved to find R provided p_B is known. It is assumed (Brennen 1995) that a bubble contains some quantity of contaminant gas whose partial pressure is p_{go} at a certain bubble reference size, R_o, and some water vapour. The water vapour pressure, p_v, is constant at a constant temperature, and the gas is assumed to be incondensable so that the gas partial pressure, p_g, can be expressed as

$$p_g=p_{go}\left(\frac{R_o}{R}\right)^{3k}. \tag{2}$$

Brennen (1995), Plesset & Prosperetti (1977), Chahine (1994), Csanady (1964) used the following expression for the pressure in a bubble

$$p_B=p_v+p_g=p_v+p_{go}\left(\frac{R_o}{R}\right)^3. \tag{3}$$

Next, consider the liquid pressure p_∞. This is a vital parameter because it is the variation of p_∞ that causes bubbles to grow or collapse. However, there is no direct or exact expression for p_∞. For convenience, some have assumed a simple function for it. For example, Prosperetti (1994) suggests the form of $p_o(1-\varepsilon\sin\omega t)$ where ε is the amplitude of oscillation, ω its frequency and t is time. Shima & Tsujino (1994) used the form of $p_\infty=p_o(1+A\sin\omega t)$ where A is the amplitude of oscillation. Much work has been done solving the bubble dynamic equation to investigate the phenomenon of cavitation (i.e. Chahine 1994; Lauterborn, Eick & Philipp 1994; Brennen 1995; Gong & Hart 1999; Wang & Brennen 1999). Most of these works assumed that the pressure takes a harmonic function and a small value of amplitude. Since these pressure amplitudes are neither from measurement nor from calculation for a real flow, the results obtained have difficulty explaining cavitation related phenomena such as the bubble cloud size and erosion ability of a cavitating water jet. In this paper, the pressure distribution in a convergent–divergent nozzle to give p_∞ is calculated using the commercial code, FLUENT, with the RNG $k-\varepsilon$ turbulence model. Once p_∞ is determined, the Rayleigh–Plesset equation, equation (1), can be solved numerically.

3. Solution of the Rayleigh–Plesset equation

The numerical solution of the Rayleigh–Plesset equation can be obtained without difficulty while the variation of pressure inside and outside the bubble is small so

Density ρ (kg m^{-3})	996
Viscosity μ (Pa s)	0.798×10^{-3}
Surface tension σ (N m^{-1})	0.072
Vapour pressure p_v (MPa)	0.00424

TABLE 1. Water properties at 300 K (Vargaftik *et al.* 1996).

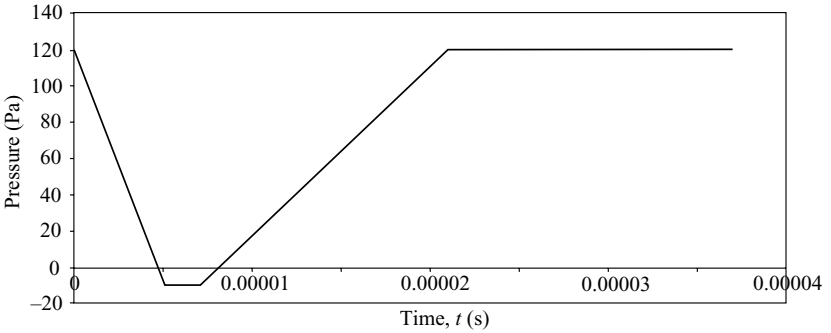

FIGURE 2. Pressure profile for testing numerical methods.

that the ratio of the maximum to minimum bubble radius is not too large. Previously published simulations fall into this category. Moss *et al.* (1994, 1997) simulated bubbles with a maximum to minimum bubble ratio of only 150. In the present work, this ratio is up to 200 000, for which standard numerical schemes experience difficulty. Lohse (2005) claims that the solution has a singularity. In the present work, while standard methods such as the adaptive Runge–Kutta method could have been used, the simple Euler method with variable time steps was used in which the iteration interval Δt varies with the bubble radius R by using the radius change as the criterion for step size.

Assuming p_B and p_∞ and the initial conditions R_o and $\dot{R}_o$ are known, then by solving (1) for the bubble radius R, the size of a bubble can be determined from its initial growth to its final collapse as a function of time. In (1), p_B includes p_g and p_v. The process of the incondensable gas inside a bubble is complicated and a heat transfer model including conduction and radiation effects will be proposed later in this paper. Here, for the purpose of testing the numerical methods, the pressure inside the bubble, p_B, is simply assumed to take the form of (3).

There is no direct or exact analytical expression for p_∞. It may be determined from practical experiments or numerical calculations. In the current investigation, the value of p_∞ is either set as a function or taken from CFD results of the simulations of nozzle flows. It is assumed that the bubble is in water at a temperature of 300 K which stays constant. The water properties are given in table 1.

Using the pressure profile in figure 2 with a variable time step based on the change of bubble size of successive time steps of $(R_i - R_{i-1})/R_{i-1} \leqslant 0.05$, the solution in figure 3 was obtained. The sharp collapse phase is captured and the solution is stable, thus allowing many rebound cycles to be computed.

4. A heat transfer model for simulating cavitation bubble

In the previous section, for the purpose of developing the numerical method for solving the Rayleigh–Plesset equation, the isothermal process is assumed. This

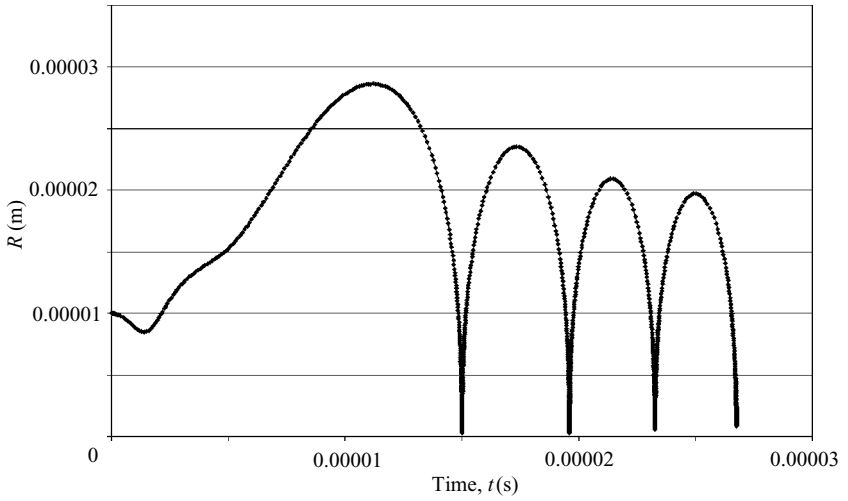

FIGURE 3. Time history of the bubble radius from the variable time step method for the pressure variation of figure 2, $R_o = 0.00001$ m and $\dot{R}_o = 0\,\mathrm{m\,s^{-1}}$.

assumption may not be true in the real case of a collapsing bubble. In this section, a more general heat transfer model is established for calculating the pressure inside the bubble, p_B.

In the Rayleigh–Plesset equation, as mentioned in the previous section, p_B represents the pressure inside the bubble which can be considered as two components, the partial pressures of vapour and incondensable gas, equation (3). The effects of condensation of vapour and evaporation of water on temperature have been analysed by Plesset (1949), who concluded that the temperature changes due to the condensation and evaporation are insignificant. It is assumed, therefore, that the process is at constant vapour pressure, p_v.

The determination of the pressure of the incondensable gas is more complicated. If the bubble growth and collapse are treated as an equilibrium thermal process, the gas pressure takes the polytropic form, equation (2). $k = 1$ implies an isothermal process and $k = \gamma = C_P/C_V = 1.4$ implies an isentropic process when the gas phase is air.

Some workers (for example Shima, Tomita & Ohno 1988) assume that the bubble collapse is an isothermal process, i.e. uniform temperature within the liquid and within the bubble. Others consider that the collapse is so violent in the final stage that the isothermal assumption would not be justified. Instead, it is more likely to be an adiabatic process. Bogoyavlenskiy (1999) assumed an adiabatic process when simulating the collapse process of an air bubble in water caused by a sound wave.

Neither the isothermal nor the isentropic process can describe accurately the whole process of the bubble growth and collapse. One might think that a polytropic model with constant k between 1 and γ will describe the process. However, this is not true if the whole process of the bubble collapse is considered. When the bubble is in its larger size phase, the process may be close to isothermal because the speed of growth and collapse is relatively slow. When the bubble is in its smaller size phase, the process may be close to adiabatic owing to the extremely fast speed of collapse. This means that a model with a constant value for k is not able to describe the whole process. We must analyse the process taking into account all possible thermal effects, that is, the effects of conduction, convection and radiation. Fujikawa & Akamatsu

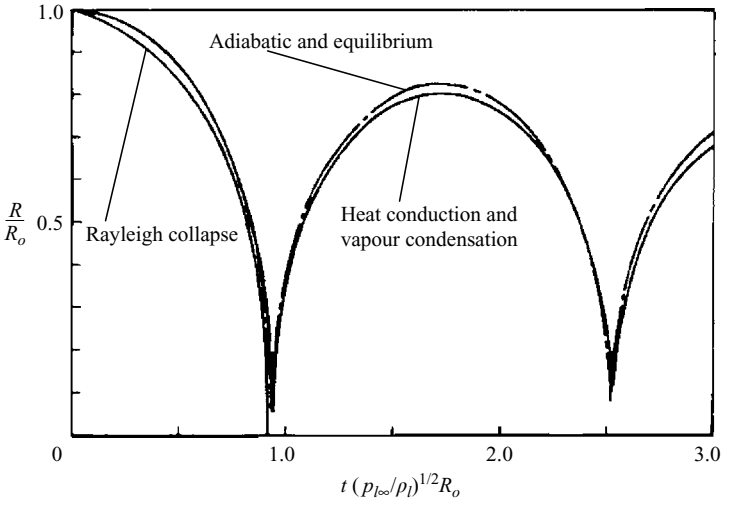

FIGURE 4. Time history of the bubble radius from the adiabatic model and a heat conduction model (after Fujikawa & Akamatsu 1980).

(1980) took into consideration the effect of vapour condensation inside the bubble and the heat conduction in which they assumed the thermal layers developing both inside and outside the bubble are thin compared with the bubble radius, but they did not consider the process of radiation which is of most concern in this section. Also, the results of Fujikawa & Akamatsu (1980) (figure 4) indicate that the vapour condensation and heat conduction do not play an important role because there is no significant difference in the time history of the bubble radius when compared with the adiabatic process.

On the other hand, it has been found that during the collapse of a cavitation bubble, light is emitted through the phenomenon of luminescence (Marinesco & Trillat 1933). When the cavitation bubble field is observed in total darkness with a dark-adapted eye (after 10–15 min), light can be seen emanating from the liquid, often in the form of filaments (Lauterborn & Ohl 1997). The faint light emitted can also be photographed with a camera equipped with a micro-channel plate as 'light intensifier'. The measurements of the spectrum of sonoluminescence by Taylor & Jarman (1970) and Flint & Suslick (1991) suggest that a temperature of 5000 K is reached in the bubble during collapse. Experiments by Barber & Putterman (1991) indicate a much higher temperature in a very short duration of the order of picoseconds. Flannigan & Suslick (2005) measured a temperature as high as 15 000 K in a single bubble containing argon in concentrated aqueous sulfuric acid solutions. Therefore, a thermodynamic model with the consideration of radiation seems to be essential.

It is generally agreed that the luminescence is due to the extremely high temperature when the bubble collapses to near its minimum size (Hilgenfeldt, Grossmann & Lohse 1999; Lohse 2005). The high temperatures and the power emissions during collapse have been predicted numerically with various assumptions (Jarman 1960; Wu & Roberts 1993, Moss *et al.* 1994). Moss *et al.* (1994, 1997) used a two-step model to simulate a bubble collapse and explained the picosecond-long sonoluminescence. The second step of their model simulates the final stage of the bubble collapse, in which a sophisticated equation constructed from a combination of data and theory is employed to describe the air state inside the bubble, including dissociation, ionization

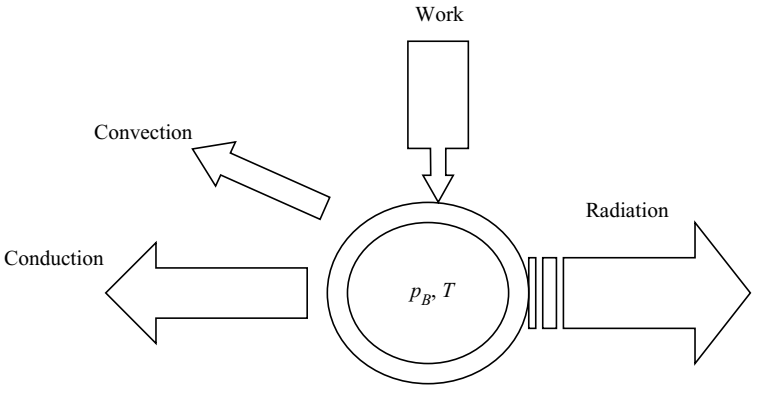

FIGURE 5. Scheme of thermal analysis of a cavitation bubble system.

and intermolecular potentials. However, the energy loss due to the radiation and thermal conduction of the surrounding water is not included. This may be why they predicted long 'tails' of high temperature which are contrary to experimental evidence. If an isentropic compression is assumed, the bubble would rebound to a large size in an unending series of cycles and never disappear owing to lack of energy dissipation.

In the present work, the purpose of simulation of the cavitation bubble is to predict when and where the bubble size decreases to the point where it eventually disappears in order to allow the determination of the bubble cloud range in the water jet. Towards this end, it is assumed that single bubble behaviour is not unlike that of a collection of bubbles, that is, bubble interaction is assumed negligible.

4.1. *Thermal analysis of the process of a bubble growth and collapse*

When a cavitation bubble grows and then collapses, the vapour inside the bubble evaporates or condenses while the pressure inside the bubble does work. When the bubble radius is around its maximum value, the work done by the pressure on the bubble system is so small that it can be ignored. However, when the bubble radius is close to its minimum value, the work done would be significant and a process of rapid heat transfer would occur.

Consider a system of a bubble surrounded by liquid (figure 5). At an instant of time, t_i, the pressure and temperature inside the bubble are p_B and T, respectively. After a finite time step Δt, the change of volume of the bubble is ΔV. The work done on the bubble is

$$w_i = -p_B \Delta V. \tag{4}$$

During this short time process, the possible ways of energy transfer between the bubble and the surrounding liquid include conduction, convection and radiation (figure 5). Considering that the velocity of the bubble relative to the surrounding liquid is small compared to the velocity of the bubble wall during collapse, we ignore the convection effect. The heat losses by conduction and radiation are $\mathrm{d}Q_{cond}$ and $\mathrm{d}Q_{rad}$.

After this short time interval, Δt, the net energy, ΔU, gained by the contents of the bubble is given according to the first law of thermodynamics as

$$\Delta U = -p_B \Delta V - \mathrm{d}Q_{cond} - dQ_{rad}. \tag{5}$$

This net energy will make the temperature of the gas in the bubble increase by ΔT given by

$$\Delta T = \frac{\Delta U}{nC_V}, \tag{6}$$

where n is the number of moles and C_V is the specific heat of the gas at constant volume.

For diatomic gases such as oxygen and nitrogen, which are dominant in the air, the specific heat is $C_V = 20.8\,\mathrm{J\,mol^{-1}\,K^{-1}}$. The number of moles n can be determined from the original volume and temperature of the bubble.

Once ΔT is obtained by (6), the temperature of the gas after the finite time, Δt, becomes

$$T_i = T_{i-1} + \Delta T. \tag{7}$$

Heat loss by conduction is given by

$$\mathrm{d}Q_{cond} = -\kappa A \nabla T\,\mathrm{d}t. \tag{8}$$

For simplification, the formula for heat transfer between two plane surfaces is used. The rate of conduction heat transfer is, therefore, calculated from

$$\mathrm{d}Q_{cond} = \frac{\kappa A(T_B - T_\infty)}{d}\Delta t, \tag{9}$$

where κ is the thermal conductivity of the water surrounding the bubble. A is the area of the bubble and d is the distance between the two surfaces. For water at 20 °C, $\kappa = 0.6\,\mathrm{Wm^{-1}\,K^{-1}}$.

The area of the bubble surface is $4\pi R^2$. However, the thickness of the water layer, d, is not easy to determine. Since the bubble radius varies during collapse, a constant value for d is not appropriated. Instead, a value that is proportional to the radius R may be reasonable. For the purpose of investigating the significance of the layer thickness, a range of $d = (0.1\text{–}1)R$ is assumed. Fortunately, as shown in §4.2, the variation of the predicted bubble collapse and rebound size is not significant when d takes values within $(0.1\text{–}1)R$ once the effect of radiation is included. For convenience of calculation, the layer thickness is taken as equal to R.

Radiation is heat transfer emitted by the bubble in a small time step, Δt, and can be written as

$$\mathrm{d}Q_{rad} = e\sigma A\left(T_B^4 - T_\infty^4\right)\Delta t, \tag{10}$$

where σ is the Stefan–Boltzmann constant. $\sigma = 5.6703 \times 10^{-8}\,\mathrm{W\,m^{-2}\,K^{-4}}$ and e is the emissivity of the hot surface. When the surface of a bubble is water, the emissivity is taken to be 0.95.

Substituting (5), (9) and (10) into (6), results in

$$\Delta T = \frac{1}{nC_V}\left[-p_B\Delta V - \frac{kA(T_B - T_\infty)}{d}\Delta t - e\sigma A\left(T_B^4 - T_\infty^4\right)\Delta t\right]. \tag{11}$$

This represents the temperature change of the bubble contents during Δt. The temperature of the bubble contents in finite-difference form becomes

$$T_i = T_{i-1} + \Delta T = T_{i-1} + \frac{1}{nC_V}\left[-p_B\Delta V - \frac{kA(T_B - T_\infty)}{d}\Delta t - e\sigma A\left(T_B^4 - T_\infty^4\right)\Delta t\right]. \tag{12}$$

Assuming perfect gas behaviour for the gas inside the bubble yields

$$p_{B_i} = p_o \frac{R_o^3}{R_i^3} \frac{T_i}{T_o}. \tag{13}$$

Substituting this into the Rayleigh–Plesset equation enables numerical solution for the cavitation bubble radius including the thermodynamics.

4.2. *Comparison of various thermal models for cavitation bubble simulation*

As outlined in the previous section, the gas partial pressure p_g plays a vital role in the final stage of collapse. The following are some numerical results that show bubble dynamic behaviour with different models for gas partial pressure. The models include isothermal, adiabatic, conduction, radiation and conduction plus radiation models. In all of the models, the partial pressure of vapour is assumed to stay constant.

Model one – isothermal:

$$p_{gi} = p_{go} \frac{R_o^3}{R_i^3}. \tag{14}$$

Model two – adiabatic:

$$p_{gi} = p_{go} \left(\frac{R_o}{R_i} \right)^{3k}, \quad k = \gamma = \frac{C_P}{C_V} = 1.4. \tag{15}$$

Model three – conduction:

$$p_{g_i} = p_o \frac{R_o^3}{R_i^3} \frac{T_i}{T_o} = p_o \frac{R_o^3}{R_i^3} \frac{1}{T_o} \left\{ T_{i-1} + \frac{1}{nC_V} \left[-p_B \Delta V - \frac{kA(T_B - T_\infty)}{d} \Delta t \right] \right\}. \tag{16}$$

Model four – radiation:

$$p_{g_i} = p_o \frac{R_o^3}{R_i^3} \frac{T_i}{T_o} = p_o \frac{R_o^3}{R_i^3} \frac{1}{T_o} \left\{ T_{i-1} + \frac{1}{nC_V} \left[-p_B \Delta V - e\sigma A \left(T_B^4 - T_\infty^4 \right) \Delta t \right] \right\}. \tag{17}$$

Model five – conduction plus radiation:

$$\begin{aligned} p_{g_i} &= p_o \frac{R_o^3}{R_i^3} \frac{T_i}{T_o} \\ &= p_o \frac{R_o^3}{R_i^3} \frac{1}{T_o} \left\{ T_{i-1} + \frac{1}{nC_V} \left[-p_B \Delta V - \frac{kA(T_B - T_\infty)}{d} \Delta t - e\sigma A \left(T_B^4 - T_\infty^4 \right) \Delta t \right] \right\}. \end{aligned} \tag{18}$$

Figure 6 presents the time history of the radius of a collapsing bubble simulated by different models. Two values for the conduction-layer thickness, d, are used. The bubble is assumed to have its maximum radius of 2.2 mm, which expanded from a micro bubble with an original radius of 0.5 μm. An ambient pressure of 0.1 MPa is assumed for p_∞ in the Rayleigh–Plesset equation. It can be seen from figure 6 that identical results are obtained in the first cycle of collapse for all the models. However, differences appear in the rebound cycles. The maximum rebound radius reached by the isothermal model is very small owing to the constant-temperature process inside the bubble. On the other hand, the adiabatic model predicts the largest rebound radius. The real rebound radius must be between the predictions by the adiabatic and the isothermal models. It is expected that the conduction plus radiation model is likely to give results close to the real case. The model data (figure 6) also show the significance of the conduction layer. It can be seen that the thickness of the conduction layer has a small effect on the end results and could be changed to improve the fit between model and experimental data.

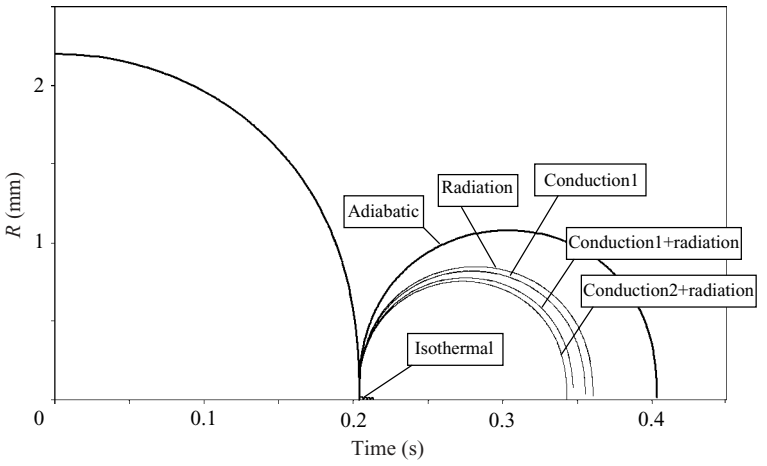

FIGURE 6. Time history of bubble radius by different thermal dynamic models (Conduction1: $d = R$; Conduction2: $d = 0.1R$).

4.3. *Comparison of numerical and experimental results*

The only way to examine the above models is to compare the numerical and experimental results. During a bubble collapse, the time history of the bubble radius is a direct indicator that can be observed. Using high-speed photography, Vogel, Lauterborn & Timm (1989), Tomita & Shima (1990) and Philipp & Lauterborn (1998) were able to take photos of collapsing bubbles with a maximum framing rate of one million frames per second. Because of the limit of the available experimental data, only three cases of bubble photos are chosen to compare with the numerical models. Of the three cases, data of Vogel *et al.* (1989) were for a spherical bubble far from the boundary, and those of Tomita & Shima (1990) were for a bubble in an infinite volume of water. Non-symmetry was not observed in these two cases. Experiments by Lauterborn & Ohl (1997) were of a bubble near a wall, in which non-symmetry appeared in the rebounding stages. To reduce the effects of the non-symmetry, the equivalent radius of the bubble used by Popinet & Zaleski (2002) in conjunction with the Rayleigh–Plesset equation is employed in this paper.

The spherical bubble case far from a boundary is available from Vogel *et al.* (1989). It can be seen from figure 7, that while the rebound radii predicted by the adiabatic and the isothermal models divert significantly from the measurements, the time history of bubble radius predicted by the conduction plus radiation model fits very well with the experimental data. The uncertainty is the original size of the micro bubble. To obtain the fit in figure 7, the original radius of the micro bubble, R_o, is assumed to be 0.5 μm. The inset in figure 7 is the expansion at the moment of first collapse to its minimum size. Although in the macro view the collapse processes predicted by the three different models look identical, they are slightly different. For example, the isothermal model, due to the assumption of a constant-temperature process, delays the building up of high pressure inside the bubble and the moment of starting the rebound is delayed about 0.02 μs relative to that of the adiabatic model.

The second comparison is made with the simulations of Popinet & Zaleski (2002) which are based on a spherically symmetric bubble simulated by the Rayleigh–Plesset equation as well as a numerical model capable of simulating bubble distortion. Both models give nearly identical results, which suggests minimal effect due to change of

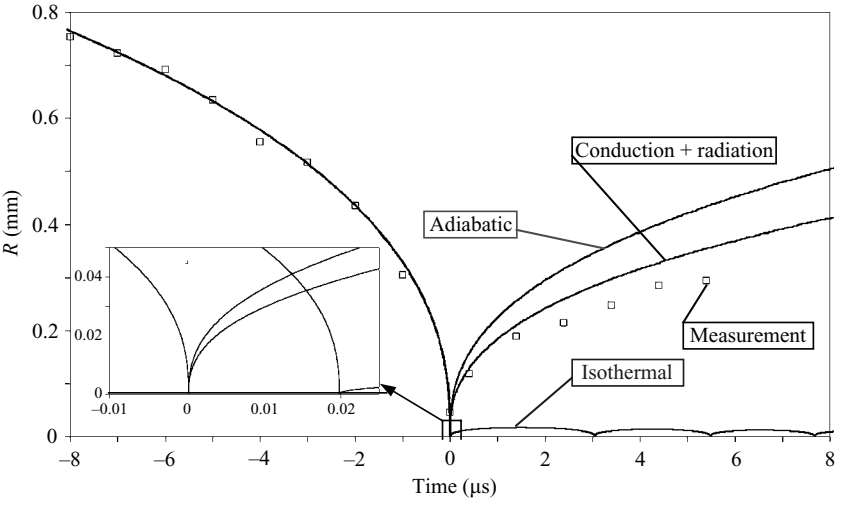

FIGURE 7. Comparison of time histories of bubble radii of different models with experimental data of Vogel *et al.* (1989).

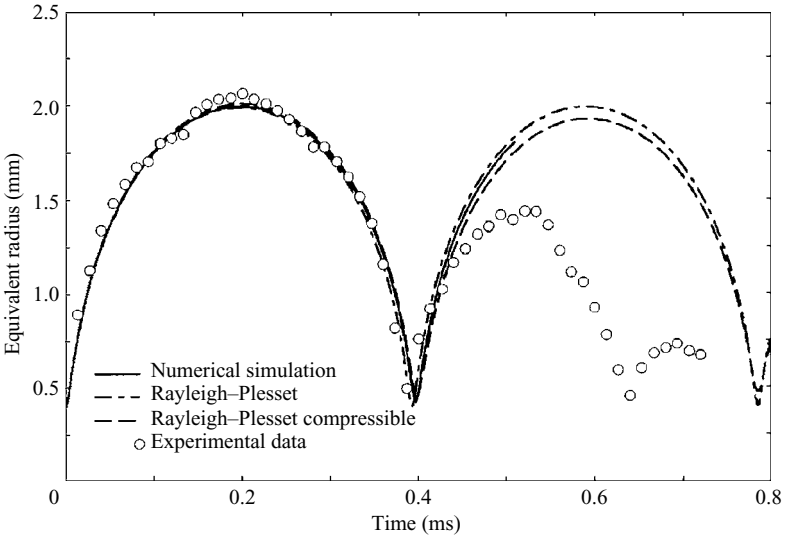

FIGURE 8. Simulations given by Popinet & Zaleski (2002), time is in ms and comparison with experimental data of Lauterborn & Ohl (1997).

bubble shape with collapse and rebound. Figure 8 shows a comparison of bubble radius predicted by Popinet & Zaleski (2002), who compared a reversible and adiabatic process for the gas pressure, with measurements by Lauterborn & Ohl (1997). In Lauterborn & Ohl's experiment, the photos show that the bubble is deformed during collapse and rebound, leading Popinet & Zaleski (2002) to measure the bubble radii in terms of an equivalent spherical bubble for comparison with predictions. Although this leads to some uncertainty for comparison with predictions owing to the tails formed during and after bubble collapse, it is seen that the models used by Popinet & Zaleski (2002) reflect neither the damping of the maximum radius of the bubble during expansion nor the changed period for the second collapse. Other uncertainties

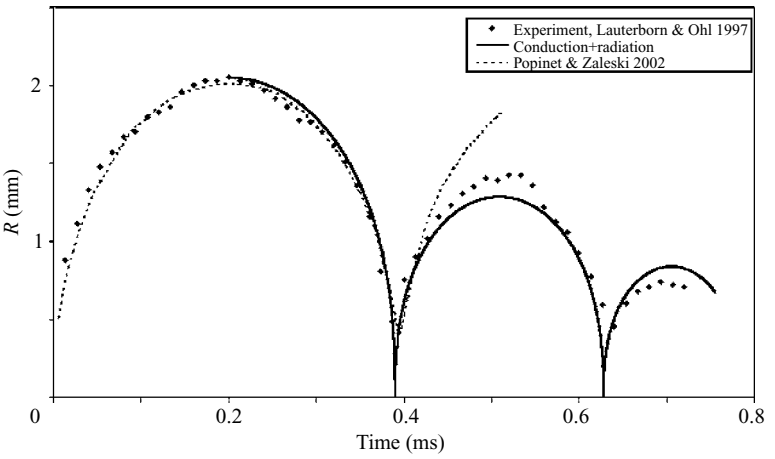

FIGURE 9. Comparison of radius predicted by the conduction plus radiation model with the measurement (assume $R_o = 30\,\mu\text{m}$).

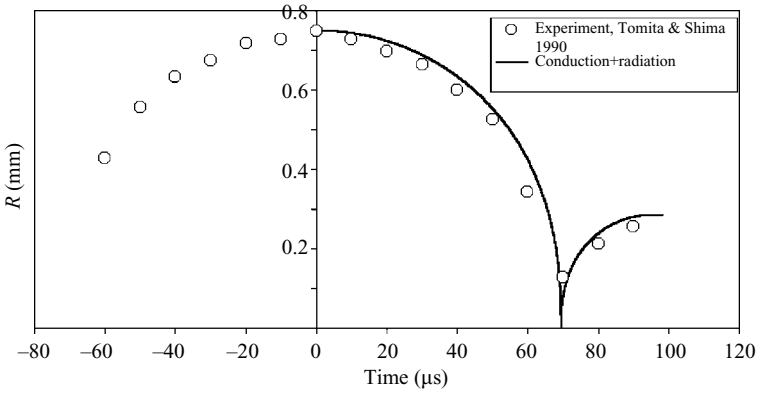

FIGURE 10. Comparison of bubble radius predicted by the conduction plus radiation model with the experimental data. (assume $R_o = 0.3\,\mu\text{m}$).

already noted by Popinet & Zaleski (2002) include the choice of initial conditions and the thermodynamic model.

Using the conduction plus radiation model developed in this section, the process of the collapse of a bubble with a maximum radius the same as in figure 8 is simulated. The predicted variation of the bubble radius is shown in figure 9, including the measurement data. The bubble is assumed to have an original radius of 30 μm. It should be noted that the conduction plus radiation model has improved the prediction up to and including the second rebound cycle.

Another comparison is made with the experimental work reported by Tomita & Shima (1990) (figure 10) who give the case of a spherical bubble in an infinite body of water. Again, the figure shows good agreement between the predicted and the experimental data when assuming an original radius of 0.3 μm which was selected to give the best fit.

In the above three cases of comparison, three different values (0.5, 30, 0.3 μm) were assumed for the original radius for the micro bubbles. Although by adjusting the

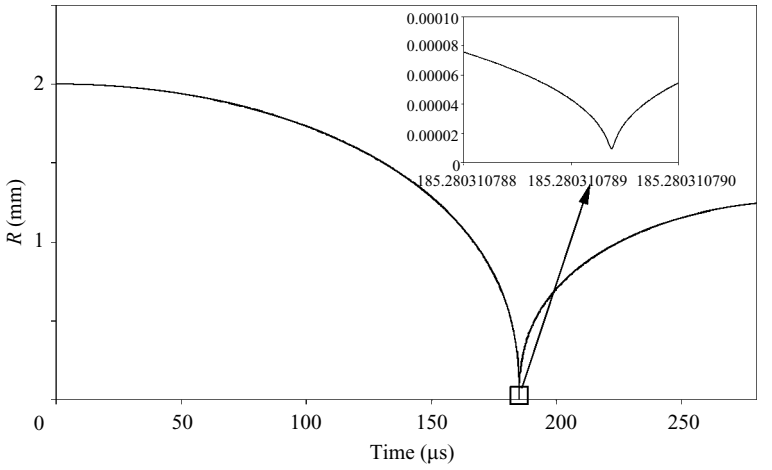

FIGURE 11. The time history of a cavitation bubble predicted by the conduction plus radiation model. The inset shows the non-singular details of the function.

power of the laser beam, the maximum size of the bubble generated can be controlled in the experiments of laser beam generated bubbles, it is impossible to know the size of the original bubble from which the cavitation bubble is generated since the range of the size of micro bubbles in water is quite large (Bennen 1995). In the case of laser produced bubbles, we cannot expect to focus the laser beam on micro bubbles with the same size every time. The need for different values of the original bubble radius for reaching desirable agreement between simulations and measurements indeed implies that these laser produced cavitation bubbles are generated from micro bubbles with different sizes.

4.4. *Bubble behaviour at the moment of minimum size*

In the above section, the bubble is simulated using the conduction plus radiation model, and the predicted bubble radii are seen to agree very well with the experimental data provided the correct initial radius is selected. During the simulation, other parameters such as the pressure and temperature inside the bubble and the velocity of the bubble wall in the bubble dynamics equation are also obtained. The variations of these parameters, may give insight into the complicated process of bubble collapse, especially to the rapidity with which it collapses to its minimum size.

Figure 11 shows the time history of the radius of the bubble simulated by the conduction plus radiation model in figure 9 where the variation of the bubble radius has been shown to match the experimental data. The bubble is assumed to be expanded by an impulse of energy to its maximum radius of 2 mm from a micro air bubble with an original radius of 30 μm and at ambient temperature. It can be seen from figure 11 that the bubble radius reaches its minimum value of about 0.01 μm at $t = 185.28$ μs. The velocity of the bubble wall at that moment, $\mathrm{d}R/\mathrm{d}t$, is shown in figure 12 and is seen to be extremely high.

Figure 13 shows the predicted temperature inside the bubble at the moment of minimum size (0.01 μm). The high temperatures have also been calculated by previous workers studying sonoluminescence, which led to a number of suggestions to explain the phenomenon, such as creation of plasma of ions, neutral atom and electrons (Apfel 1999; Hilgenfeldt *et al.* 1999; Flannigan & Suslick 2005; Lohse 2005). Although a

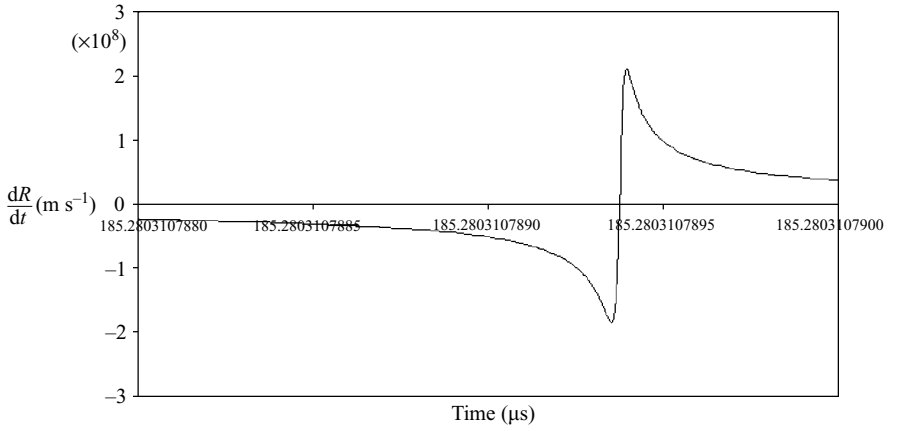

FIGURE 12. Wall velocity of a collapsing bubble at the moment of minimum size.

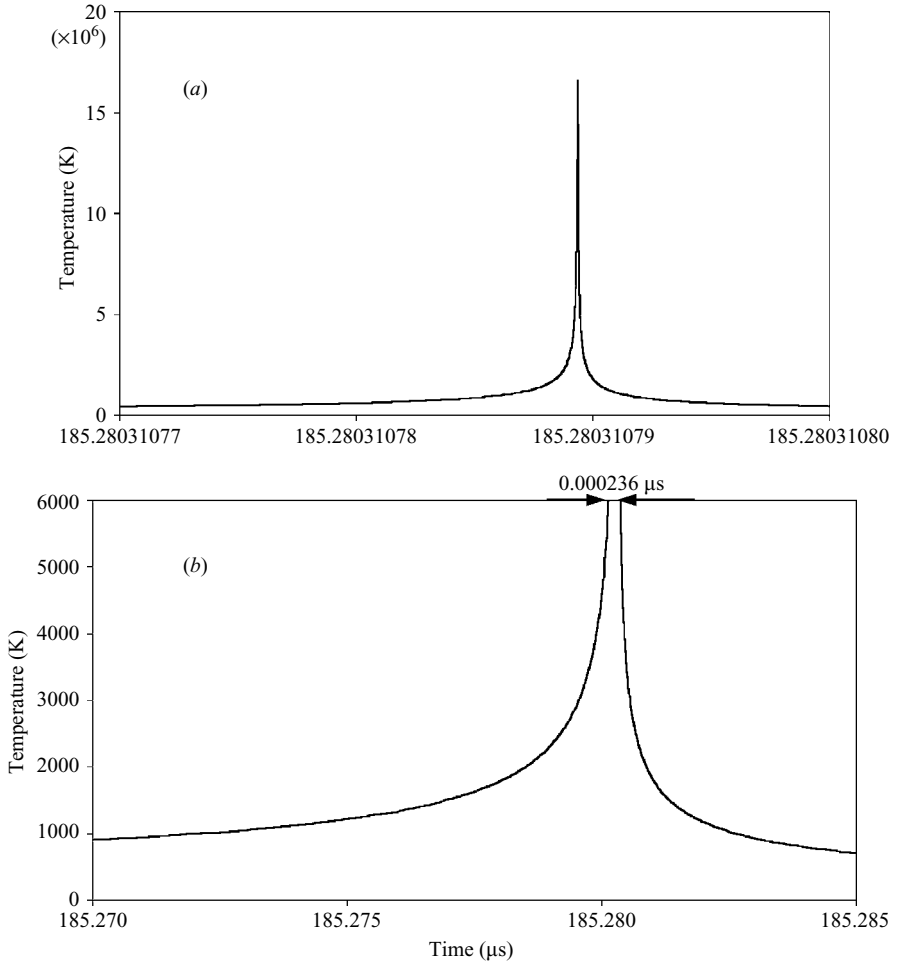

FIGURE 13. Temperature inside the bubble at the moment of minimum size.

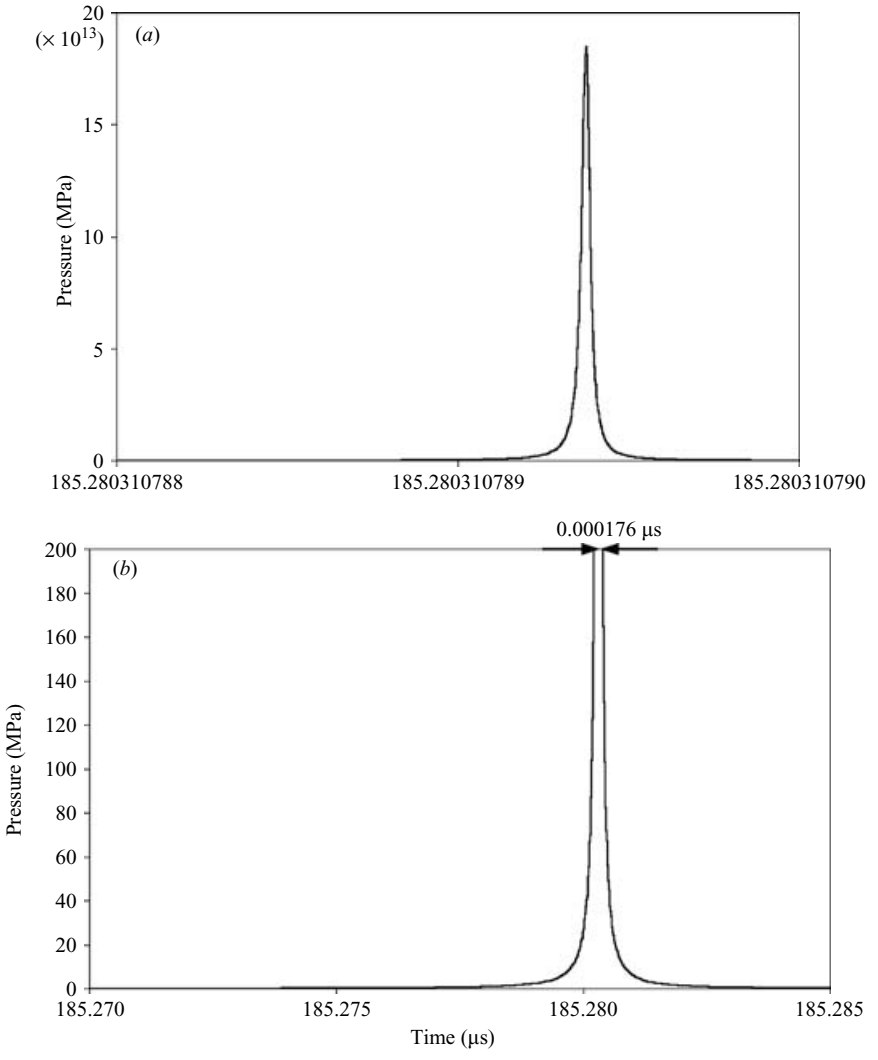

FIGURE 14. Pressure inside the bubble at the moment of minimum size.

temperature as high as 15 200 K has been deduced through measurement of light emission from an argon bubble submerged in sulfuric acid solution (Flannigan & Suslick 2005), the calculated maximum temperature in figure 13 is still believed to be unrealistic. Possible reasons for this include assumptions such as constant specific heat and applicability of the perfect gas equation of state which would not be valid at such a high temperature. However, since the duration of high temperature is extremely small, it may not affect the simulation of the whole processes of collapse and rebound of a bubble, particularly, if it is radiation related and hence responds as temperature to the fourth power. For example, the duration of higher than 6000 K is only 0.236 ps which agrees with the experimental results that the width of the light emission spike is less than 50 ps (Barber & Putterman 1991). A similar result is obtained for the pressure inside the bubble (figure 14).

5. Modelling the pressure outside of the bubble

In the Rayleigh–Plesset equation, in addition to the pressure p_B inside the bubble, which was discussed in the previous section, there is another important variable, the pressure outside the bubble denoted by p_∞. The expansion and collapse of a bubble are determined by the relative variation of these two pressures. In the case of the laser-produced cavitation, as simulated in the previous section, the cavitation bubble is caused by the highly focused energy of the laser beam assuming the outside pressure remains unchanged. However, in the case of a cavitating water jet, the outside pressure is the driving force for cavitation rather than the energy from a laser beam. In this case, cavitation occurs only when the outside pressure p_∞ reduces to below the vapour pressure. When p_∞ recovers to values above the vapour pressure, the bubble starts to collapse. So it is essential to know the pressure variation in the water jet.

In the domain of a water jet, it is assumed that the pressure field is identical to what is calculated from the CFD model. If it is assumed that a bubble travels with the jet, it experiences a pressure variation while it flows through the nozzle. The pressure profile is a function of position. To replace the pressure p_∞ outside the bubble with the calculated pressure profile, we must change the Rayleigh–Plesset equation to add position dependence because its original form is time dependent, equation (1). This can be achieved from the relationship of velocity (v) and displacement (x),

$$\Delta x = v\Delta t. \tag{19}$$

Applying the assumption of no slip for the multiphase (bubble and liquid) flow, the values of velocity of the bubble and the pressure on the bubble are those of the water flow at the corresponding position. Along any flow stream path, velocity v_i is a function of position, x_i, that is

$$v_i = v(x_i). \tag{20}$$

From (19) and (20),

$$\Delta t = (x_i - x_{i-1})/v(x_i). \tag{21}$$

Using (21), the first- and second-order derivatives of the bubble radius of the Rayleigh–Plesset equation can be written in backward difference form as:

$$\left(\frac{\Delta R}{\Delta t}\right)_i = \frac{R_i - R_{i-1}}{\Delta t} = \frac{R_i - R_{i-1}}{(x_i - x_{i-1})/v(x_i)}, \tag{22}$$

$$\left(\frac{\Delta^2 R}{\Delta t^2}\right)_i = \frac{\left(\frac{\Delta R}{\Delta t}\right)_i - \left(\frac{\Delta R}{\Delta t}\right)_{i-1}}{\Delta t} = \frac{\left(\frac{\Delta R}{\Delta t}\right)_i - \left(\frac{\Delta R}{\Delta t}\right)_{i-1}}{(x_i - x_{i-1})/v(x_i)}$$

$$= \frac{\left(\frac{R_i - R_{i-1}}{(x_i - x_{i-1})/v(x_i)}\right) - \left(\frac{R_{i-1} - R_{i-2}}{(x_{i-1} - x_{i-2})/v(x_{i-1})}\right)}{(x_i - x_{i-1})/v(x_i)}. \tag{23}$$

Similarly, the pressure, p_i, is also a function of position, x_i, that is

$$p_i = p(x_i). \tag{24}$$

Replacing $p_{\infty i}$ with $p(x_i)$ and substituting equations (21) to (24) in the Rayleigh–Plesset equation (1), the required finite-difference equation in the position-dependent form is obtained.

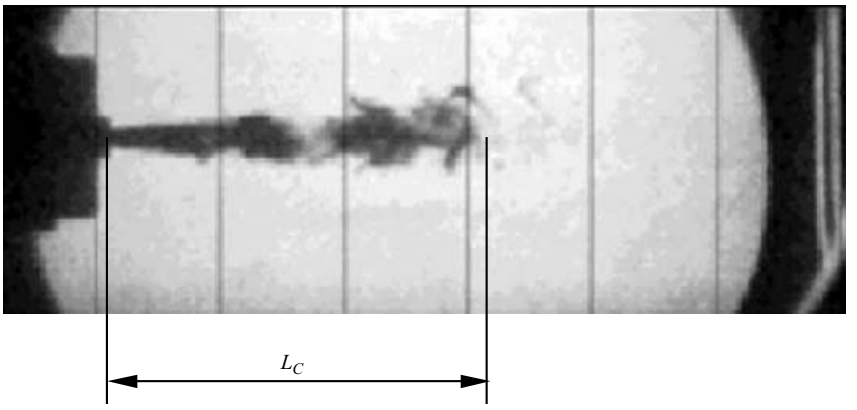

FIGURE 15. A typical bubble cloud in a cavitation water jet.

$$\rho\left[R_i\left(\frac{\left(\frac{R_i-R_{i-1}}{(x_i-x_{i-1})/v(x_i)}\right)-\left(\frac{R_{i-1}-R_{i-2}}{(x_{i-1}-x_{i-2})/v(x_{i-1})}\right)}{(x_i-x_{i-1})/v(x_i)}\right)+\frac{3}{2}\left(\frac{R_i-R_{i-1}}{(x_i-x_{i-1})/v(x_i)}\right)^2\right]$$
$$=p_B-p\,(x_i)-\frac{2\sigma}{R}-\frac{4\mu}{R}\frac{R_i-R_{i-1}}{(x_i-x_{i-1})/v(x_i)}. \tag{25}$$

With $p(x_i)$ and $v(x_i)$ being calculated, a program written according to (25) is able to give a solution that describes the variation of the bubble radius versus position. However, since the calculated data are only on the nodes, the position, x_i, in (25) may not be coincident with the node positions when using variable step length which is needed for solving the Rayleigh–Plesset equation. When nodes for the CFD calculation and the Rayleigh–Plesset equation are not coincident, linear interpolation is used.

6. Prediction of bubble cloud length

When the micro bubbles flowing in a water jet grow and then collapse and rebound as they travel downstream, they appear like a cloud owing to the large number of bubbles and their high velocity. The bubble cloud can be recorded photographically (Meyer *et al.* 1999; Qin 2004). After a few cycles of collapse and rebound, the maximum rebound sizes become small and eventually invisible in the photos. The length of the cloud is denoted as L_C. Figure 15 is a typical image of a bubble cloud in a cavitating water jet.

The cloud length, L_C, may be considered to be equal to the travelling distance of the bubbles from the nozzle exit to the position where they collapse to such a degree that their rebound sizes become invisible (this may be reached after several cycles of collapse and rebound). We consider that the bubble cannot be measured from the photo when the rebound radius is smaller than 0.5 mm. The distance travelled and hence L_C can be calculated by solving (25) using the pressure and velocity profiles obtained from CFD.

The simulation is for a typical nozzle used for our erosion tests. The nozzle is mounted in a cavitation cell (figures 16 and 17), so that the cavitation bubble cloud can be recorded photographically. The convergent–divergent nozzle geometric details

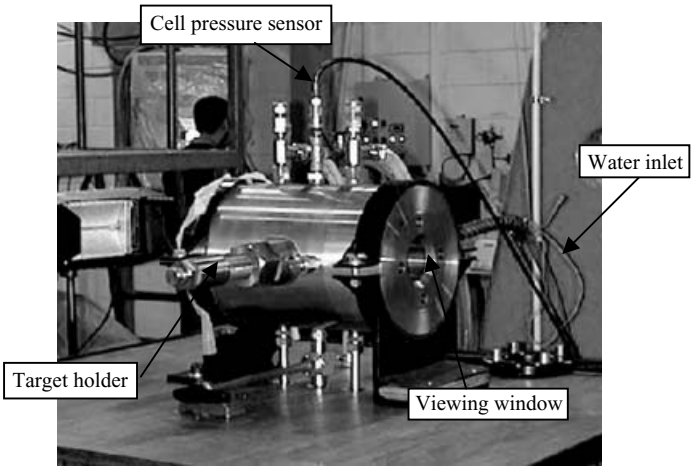

FIGURE 16. Cavitation test cell.

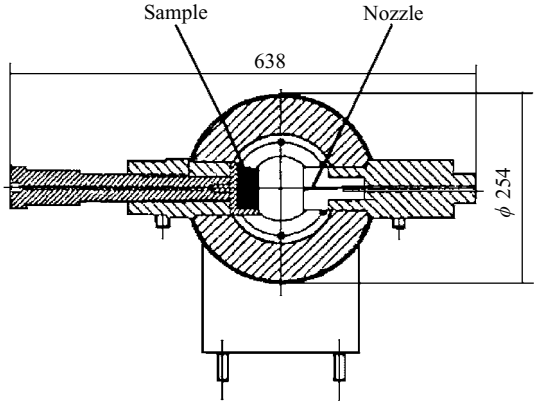

FIGURE 17. Cross-section through test cell; dimensions in mm.

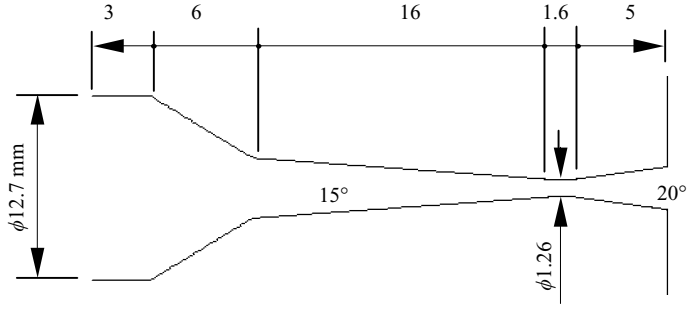

FIGURE 18. Configuration of a convergent–divergent nozzle used in the erosion tests.

are shown in figure 18. A pump pressure of 97 MPa and cell pressure of 6 MPa are applied for the water jet. For present purposes, the bubble cloud was photographed and the cloud length was measured on the photos as 27 mm (figure 19).

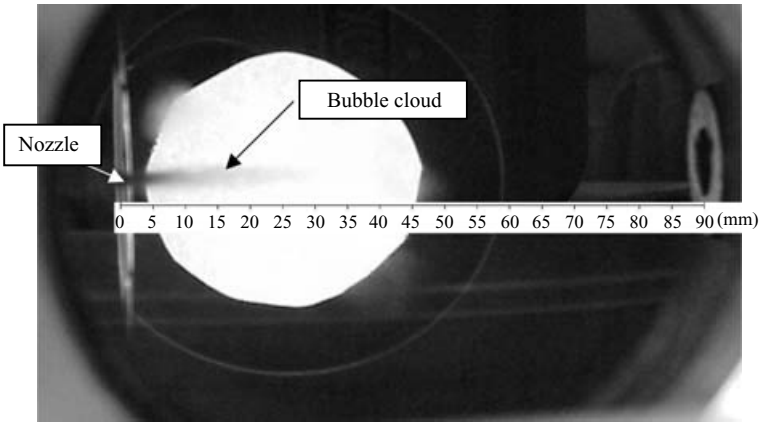

FIGURE 19. Cavitation bubble cloud in the convergent–divergent nozzle flow at 97 MPa pump pressure and 6 MPa cell pressure.

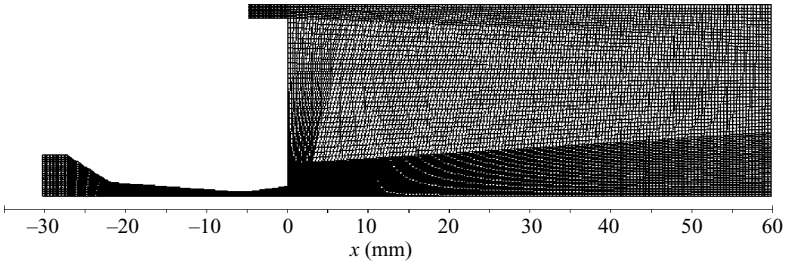

FIGURE 20. Meshed flow domain (19 666 nodes).

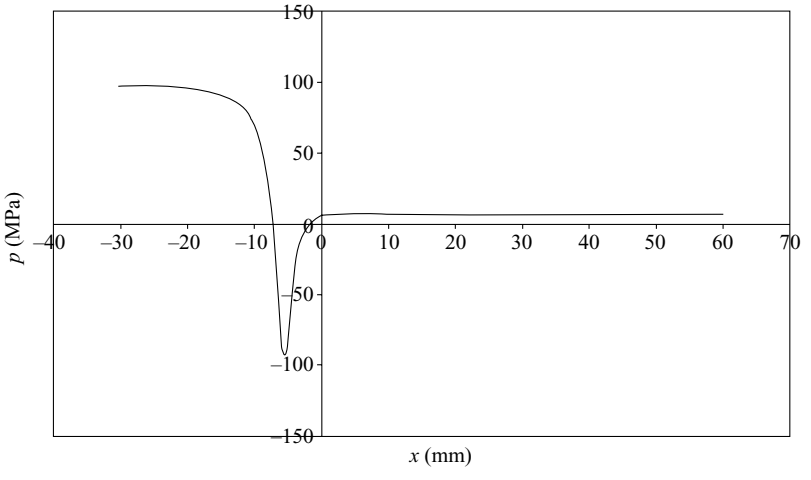

FIGURE 21. Pressure profile along the jet centreline.

The first step is to simulate the water-jet flow to obtain the pressure and velocity profiles. The meshed flow domain including the nozzle and the cavitation cell is shown in figure 20. The nozzle flow is simulated using the RNG $k-\varepsilon$ model for constant density of water within the commercial code FLUENT to obtain the pressure and velocity profiles along the centreline of the jet (figures 21 and 22). From figure 21

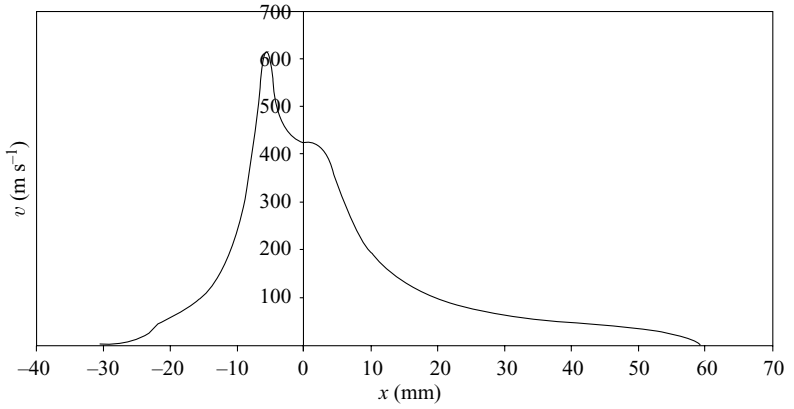

FIGURE 22. Velocity profile along the jet centreline.

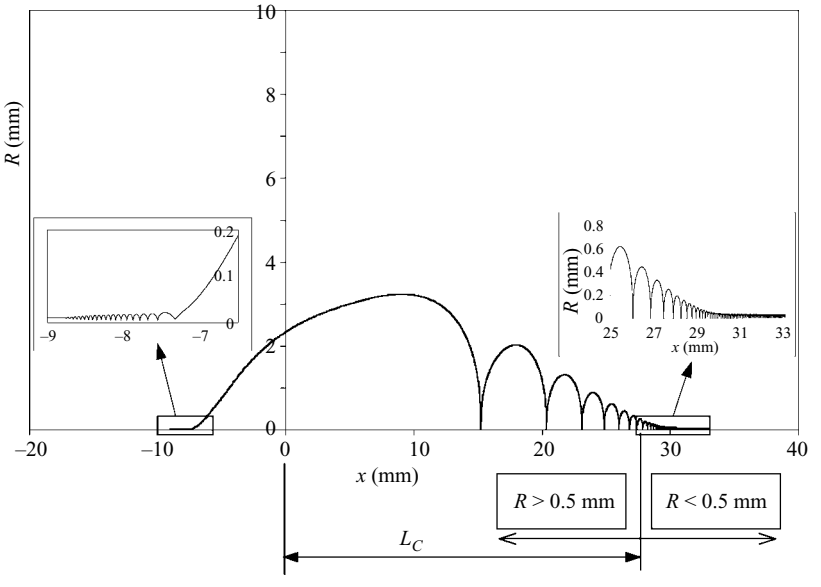

FIGURE 23. An example of bubble radius variation in a variable pressure field (assume original radius $R_o = 80\,\mu m$ at 1 atm).

it can be seen that there is a significant pressure reduction in the throat of the nozzle. The pressure then recovers to the ambient pressure (6 MPa) downstream of the nozzle. If a micro bubble goes through the nozzle, it must experience this variation of pressure leading to cavitation and collapse.

The second step of the simulation is to consider a bubble travelling along the centreline while maintaining spherical symmetry and moving without slip relative to the surrounding water. Assuming that the micro gas bubble has an initial size of 80 μm radius at 1 atm, it becomes 8 μm when it comes to the nozzle inlet (97 MPa). Using the pressure and velocity profiles as shown in figures 21 and 22, the variation of the bubble radius is calculated with the conduction plus radiation model resulting in the variation of figure 23. (A minimum time step of 2×10^{-22} s is used in this computation.)

It can be seen from figure 23 that a micro bubble oscillates with increasing amplitude when it reaches the throat as the water pressure decreases. The oscillating amplitude is of the order of 10 μm before the pressure reaches zero. However, the bubble grows rapidly at the throat (about $x = -7.3$ mm) where the water pressure reduces to a negative value. It reaches its maximum size at a distance from the nozzle exit of about 11 mm and completely finishes its first collapse at 16 mm from the exit. A sequence of rebounds and collapses follow the first collapse. Meanwhile, the maximum radius for each rebound decreases gradually and finally becomes invisible. The radius of the bubble will become its final equilibrium size of about 20 μm at the cell pressure of 6 MPa. Assuming bubbles with radius of 0.5 mm to be invisible in the bubble cloud photos, the distance L_C, from the nozzle exit to the position where the bubble radius is smaller than 0.5 mm can be considered the predicted bubble cloud length. In other words, in this case, the predicted bubble cloud length is 26–27 mm, which is close to the experimental result (27 mm) obtained from the photos of the bubble cloud under the same operating conditions (figure 19).

When solving the bubble dynamics equation, the initial bubble radius R_o at atmospheric conditions must be assumed for determining the amount of incondensable air in the bubble. This may affect the prediction of the bubble cloud length. To investigate the effect of R_o on the bubble life cycle, a series of analyses was carried out by changing R_o. We found that the distance from the exit of the nozzle to the point where the bubble finishes its first collapse is unchanged for bubbles having an original radius of 1 to 100 μm. Changing R_o just slightly affects the rebound radius and slightly changes the visible bubble cloud length L_C. For example, when R_o changes from 10 to 30 μm, the bubble cloud length L_C changes only 2.3 %. This is convenient for predicting the bubble cloud length, because one can predict bubble cloud length with satisfactory accuracy without needing to know accurately the original size of the micro bubble which has a large range and is hard to determine.

The phenomenon that the original size of bubble does not affect the first cycle of collapse can also be explained from the Rayleigh–Plesset equation, (1). The behaviour of the bubble depends on the inside and outside pressures, p_B and p_∞. In the first cycle of growth and collapse, the bubble experiences a very large negative pressure. The inside pressure which consists of incondensable air contained in the original bubble is so small compared to the magnitude of the negative pressure that its effect can be ignored. In the following sequences of rebounds, the bubble is at the cell pressure which is much smaller than the magnitude of the throat pressure. As a result, the effect of inside pressure is observed.

The life cycle of cavitation bubbles in this convergent–divergent nozzle flow can be seen more clearly if the bubble variation is plotted together with the pressure and velocity profiles (figure 24). An existing bubble does not grow when it comes into the convergent section of the nozzle owing to the high local pressure. When it approaches the throat, as the pressure reduces to below the vapour pressure, the micro bubble starts to grow. When it leaves the nozzle exit, although the pressure has recovered to the cell pressure (6 MPa), which is much higher than the vapour pressure (0.0042 MPa), the bubble does not stop growing. This is due to the effect of inertia which is controlled by the second derivative term in the Rayleigh–Plesset equation. The bubble continues growing until it reaches its maximum size at a distance of about 11 mm from the exit.

A series of simulations was conducted to predict the bubble cloud length for different operating conditions. Figure 25 presents plots of the bubble radius variation for a fixed 82 MPa pump pressure but variable cell pressures, p_c, of 1, 2, 3, 4 and

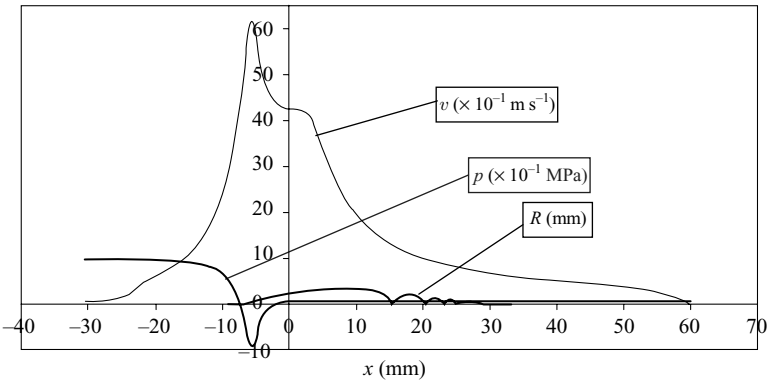

FIGURE 24. Variations of predicted pressure, velocity and radius of a bubble in a water-jet flow of the convergent–divergent nozzle.

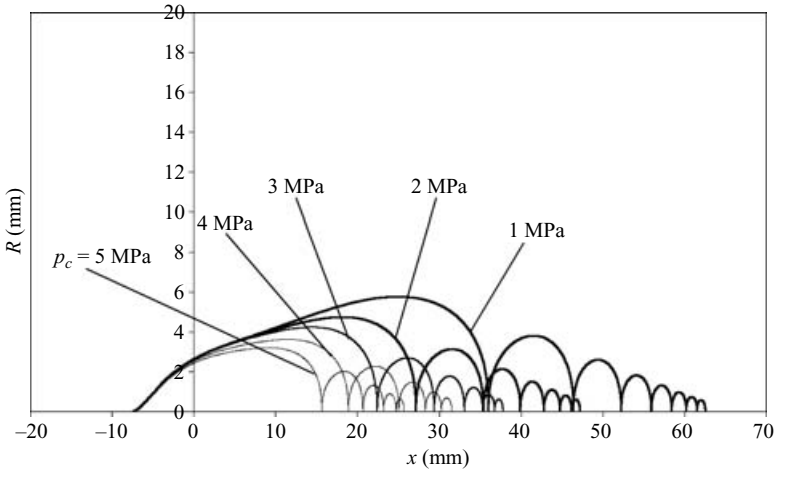

FIGURE 25. Variations of the predicted radius of a bubble in water-jet flows of the convergent–divergent nozzle at 82 MPa pump pressure but five different cell pressures (p_c represents the cell pressure).

5 MPa. The predicted bubble cloud lengths for the above cell pressures are shown in figure 26 together with measured bubble cloud length in the experiments carried out in the cavitation cell (Qin 2004).

From figure 26, it can be seen that while the predictions match experiments well for all the operating conditions, the error increases as the cell pressure (ambient pressure) decreases. The measured bubble cloud lengths are longer than the predictions when the cell pressure p_c becomes small. One of the reasons, we believe, is the cavitation bubble formation generated by pressure fluctuations associated with the turbulence. This involves a mechanism of cavitation not covered by the present model which considers only pressure variation caused by the flow path variation as the flow passes through the convergent–divergent nozzle and beyond. Computations (Qin 2004) indicate that the turbulence in this water jet can cause the amplitude of the pressure fluctuation to reach more than 2 MPa when the cell pressure is 2 MPa. This means that the turbulence of the jet can generate cavitation bubbles when the cell pressure is near 2 MPa or smaller. As a result, there are extra bubbles in the jet flow in

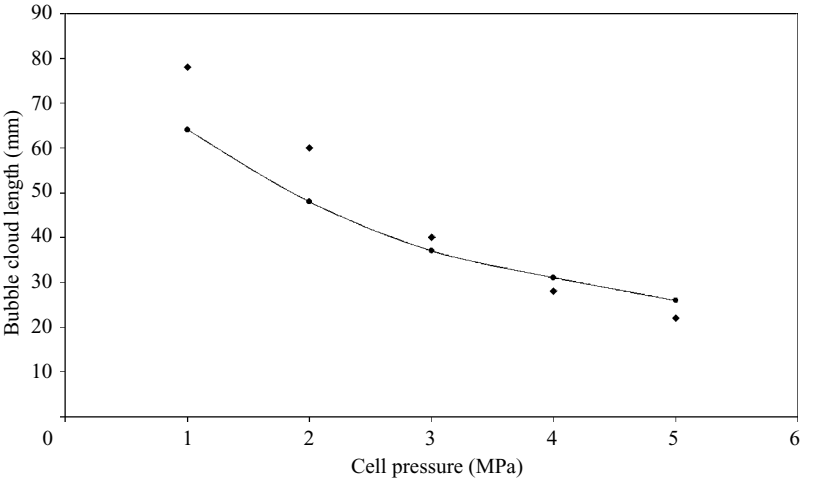

FIGURE 26. Comparison of —, the predicted and ◆, measured bubble cloud lengths with 82 MPa pump pressure and different cell pressures.

addition to those caused by the pressure reduction in the nozzle throat. Consequently, the measured bubble cloud length is longer than the prediction. Another source of difference between computation and measurement may be that the assumption of spherical symmetry is partially invalid during bubble travel.

7. Conclusions

A model is developed for simulating bubbles travelling in submerged water jets. The model uses data from CFD simulation as input to give the ambient pressure variation along the flow. In determining the inside pressure of the bubble, a thermal model which includes heat transfer by conduction plus radiation has been formulated. For achieving an accurate solution of the highly nonlinear second-order differential equation such as the Rayleigh–Plesset equation, a finite-difference variable time-step method is applied by placing a limit on the bubble radius variation from one iteration to the next.

By accounting for conduction and radiation effects, the model can determine more accurately the pressure inside the bubble during collapse than the alternative models of isothermal or adiabatic behaviour. The model also shows that radiation is the dominant heat transfer mode. The predicted variation of bubble radius agrees well with the experimental result, thus suggesting that an essential feature is a temperature to the fourth-power dependence. Consistent with many previous studies, effects such as shock waves, plasma formation during collapse, a limit on minimum bubble size, asymmetry, non-perfect gas behaviour, compressibility and acoustic emissions have been neglected.

Details of the process of the final stage of collapse and rebound can be simulated. If single bubble behaviour can be extended to behaviour of bubble clouds and including bubble behaviour near boundaries, a possible model for prediction of erosion caused by cavitation water jet may result.

Taking the distance to where the bubble becomes invisible as the calculated bubble cloud length, the predicted result for a water jet agrees with the measurement on photos of bubble clouds generated in submerged water jet. By establishing the model

for simulating bubble growth and collapse, it allows the prediction of the bubble cloud length with different nozzle geometries under different operating conditions for optimization of nozzle geometry.

This work was conducted within the Water Jet Fundamentals Program of CRC Mining. Industry support from BHP Billiton–Mitsui Alliance and Anglo Coal Australia is gratefully acknowledged.

REFERENCES

Apfel, R. 1999 And there was light. *Nature* **398**, 378–379.

Barber, B. P. & Putterman, S. J. 1991 Observations of synchronous picosecond sonoluminescence. *Nature* **352**, 318.

Bogoyavlenskiy, V. A. 1999 Differential criterion of a bubble collapse in viscous liquids. *Phys. Rev.* E **60**, 504.

Brennen, C. E. 1995 *Cavitation and Bubble Dynamics*. Oxford University Press.

Chahine, G. L. 1994 Strong interactions bubble/bubble and bubble/flow. *Bubble Dynamics and Interface Phenomena* (ed. J. R. Blake, J. M. Boulton-Stone & N. H. Thomas), pp. 195–206. Kluwer.

Csanady, G. T. 1964 *Theory of Turbomachines*. McGraw–Hill.

Flannigan, D. J. & Suslick, K. S. 2005 Plasma formation and temperature measurement during single-bubble cavitation. *Nature* **434**, 52–55.

Flint, E. B. & Suslick, K. S. 1991 The temperature of cavitation. *Science* **253**, 1397–1399.

Fujikawa, S. & Akamatsu, T. 1980 Effects of the non-equilibrium condensation of vapour on the pressure wave produces by the collapse of a bubble in a liquid. *J. Fluid Mech.* **97**, 481–512.

Gong, C. L. & Hart, D. P. 1999 Interactions of bubble dynamics and chemistry in cavitation bubbles induced by ultrasound. *Proc. 3rd ASME/JSME Joint Fluids Engineering Conf., San Francisco, USA*, pp. 1–5.

Hilgenfeldt, S., Grossmann, S. & Lohse, D. 1999 A simple explanation of light emission sonoluminescence. *Nature* **398**, 402–405.

Jarman, P. D. 1960 Sonoluminescence – A Discussion. *J. Acoust. Soc. Am.* **32**, 1459–1462.

Knapp, R. T. 1952 *Proc. Inst. Mech. Engrs Lond.* **166**, 150.

Knapp, R. T., Daily, J. W. & Hammit, F. G. 1970 *Cavitation*. McGraw–Hill.

Lauterborn, W. & Bolle, H. 1975 Experimental investigations of cavitation bubble collapse in the neighbourhood of a solid boundary. *J. Fluid Mech.* **72**, 391–399.

Lauterborn, W. & Ohl, C. 1997 Cavitation bubble dynamics. *Ultrasonics Sonochem.* **4**, 65–75.

Lauterborn, W., Eick, I. & Philipp, A. 1994 Approaching bubble dynamics with lasers, holography and computers. *Bubble Dynamics and Interface Phenomena* (ed. J. R. Blake, J. M. Boulton-Stone & N. H. Thomas), pp. 299–310. Kluwer.

Lohse, D. 2005 Cavitation hots up. *Nature* **434**, 33–34.

Marinesco, M. & Trillat, J. J. 1933 Action des ultrasons sur les plaques photographiques. *CR Acad. Sci. Paris.* **196**, 858–860.

Meyer, T., Carnavas, P., Alehossein, H., Hood, M., Adam, S. & Gledhill, M. 1999 The effect of nozzle design on erosion performance of cavitating water jets. *Intl Symp. on New Applications of Water Jet Technology, Japan*, pp. 33–41.

Moss, W. C., Clarke, D. B., White, J. W. & Young, D. A. 1994 Hydrodynamic simulations of bubble collapse and picosecond sonoluminescence. *Phys. Fluids* **6**, 2979–2985.

Moss, W. C., Clarke, D. B. & Young, D. A. 1997 Calculated pulse widths and spectra of a single sonoluminescing bubble. *Science* **276**, 1398–1401.

Philipp, A. & Lauterborn, W. 1998 Cavitation erosion by single laser-produced bubbles. *J. Fluid Mech.* **361**, 75–116.

Plesset, M. S. 1949 The dynamics of cavitation bubbles. *Trans. ASME J. Appl. Mech.* **16**, 228–231.

Plesset, M. S. & Prosperetti, A. 1997 Bubble dynamics and cavitation. *Annu. Rev. Fluid Mech.* **9**, 1451–185.

Popinet, S. & Zaleski, S. 2002 Bubble collapse near a solid boundary: a numerical study of the influence of viscosity. *J. Fluid Mech.* **464**, 137–163.

Prosperetti, A. 1994 Some things we did not know 10 years ago. *Bubble Dynamics and Interface Phenomena* (ed. J. R. Blake, J. M. Boulton-Stone & N. H. Thomas), pp. 3–16. Kluwer.

Qin, Z. 2004 Investigation of the cavitation mechanism and erosion of submerged high pressure water jets. PhD thesis, The University of Queensland, Australia.

Rayleigh, Lord 1917 On the pressure developed in a liquid during collapse of a spherical cavity. *Phil. Mag.* **34**, 94–98.

Shima, A. & Tsujino, T. 1994 The dynamics of cavity clusters in polymer aqueous solutions subjected to an oscillating pressure. *Bubble Dynamics and Interface Phenomena* (ed. J. R. Blake, J. M. Boulton-Stone & N. H. Thomas), pp. 81–92. Kluwer.

Shima, A., Tomita, Y. & Ohno, T. 1988 Temperature effects on single bubble collapse and induced impulsive pressure. *Trans. ASME* I: *J. Fluids Engng* **110**, 194–199.

Shima, A., Tomita, Y., Gibson, D. C. & Blake, J. R. 1989 The growth and collapse of cavitation bubbles near composite surfaces. *J. Fluid Mech.* **203**, 199–214.

Taylor, K. J. & Jarman, P. D. 1970 The spectra of sonoluminescence. *Austral. J. Phys.* **23**, 319–334.

Tomita, Y. & Shima, A. 1990 High speed photographic observations of laser-induced cavitation bubbles in water. *Acustica* **71**(3), 161–171.

Trilling, L. 1952 The collapse and rebound of a gas bubble. *J. Appl. Phys.* **23**, 14–17.

Vargaftik, N. B., Vinogradov, Y. K. & Yargin, V. S. 1996 *Handbook of Physical Properties of Liquids and Gases*. Begell House.

Vogel, A., Lauterborn, W. & Timm, R. 1989 Optical and acoustic investigations of the dynamics of laser-produced cavitation bubbles near a solid boundary. *J. Fluid Mech.* **206**, 299–338.

Wang, Y. C. & Brennen, C. E. 1999 Numerical computation of shock waves in a spherical cloud of cavitation bubbles. *Trans. ASME* I: *J. Fluids Engng* **121**, 872–880.

Wu, C. C. & Roberts, P. H. 1993 Shock-wave propagation in a sonoluminescing gas bubble. *Phys. Rev. Lett.* **70**, 3424–3427.

Young, F. R. 1989 *Cavitation*. McGraw–Hill.